VIRUS EVOLUTION

Virus Evolution, 2025, **11(1)**, veaf045
DOI: https://doi.org/10.1093/ve/veaf045
Advance Access Publication 27 June 2025
Research Article

Identification of a putative new virus from the *Jingmenvirus* group in ticks from wild animals in Brazil

Dayla Bott Geraldini[1], Cintia Bittar[1,2,*], Fabio Sossai Possebon[3], Carolina Gismene[4], Ricardo Barros Mariutti[4], Vivaldo Gomes da Costa[1], Guilherme Rodrigues Fernandes Campos[5], Rafael Cesário Beltrão[6], Guilherme Guerra Neto[6], Antônio Carlos Lofego[7], Mauricio Lacerda Nogueira[5], Raghuvir Krishnaswamy Arni[4], João Pessoa Araújo Junior[3], Marília de Freitas Calmon[1], Paula Rahal[1]

[1]Laboratório de Estudos Genômicos, Departamento de Biologia, Instituto de Biociências Letras e Ciências Exatas (IBILCE), Universidade Estadual Paulista (Unesp), Rua Cristóvão Colombo, São José do Rio Preto, São Paulo, 15054-000, Brazil
[2]Laboratory of Molecular Immunology, The Rockefeller University, York Ave, New York, New York, 10065, United States
[3]Instituto de Biotecnologia, Universidade Estadual Paulista (Unesp), Alameda das Tecomarias, Botucatu, São Paulo, 18607-440, Brazil
[4]Centro Multiusuário de Inovação Biomolecular, Departamento de Física, Instituto de Biociências Letras e Ciências Exatas (IBILCE), Universidade Estadual Paulista (Unesp), Rua Cristóvão Colombo, São José do Rio Preto, São Paulo, 15054-000, Brazil
[5]Laboratório de Pesquisas em Virologia, Departamento de Doenças Dermatológicas, Infecciosas e Parasitárias, Faculdade de Medicina de São José do Rio Preto (FAMERP), Avenida Brigadeiro Faria Lima, São José do Rio Preto, São Paulo, 15090-000, Brazil
[6]Zoológico Municipal de São José do Rio Preto, Avenida Nelson da Veiga, São José do Rio Preto, São Paulo, 15053-600, Brazil
[7]Laboratório de Acarologia, Departamento de Biologia, Instituto de Biociências Letras e Ciências Exatas (IBILCE), Universidade Estadual Paulista (Unesp), Rua Cristóvão Colombo, São José do Rio Preto, São Paulo, 15054-000, Brazil

*Corresponding author. Universidade Estadual Paulista (Unesp), Instituto de Biociências Letras e Ciências Exatas (IBILCE), Rua Cristóvão Colombo, 2265, Jardim Nazareth, 15054-000, São José do Rio Preto, SP, Brazil. E-mail: cintia.bittar@unesp.br

Abstract

Ticks are obligate hematophagous arthropods that can transmit pathogens and are important vectors of diseases affecting wild and domestic animals, as well as humans, thus representing a serious risk to public health. Despite the growing concern about arboviruses, our understanding of tick-borne viruses remains limited compared to those transmitted by mosquitoes. We performed metagenomic analysis, focusing on the virome of ticks collected from wild animals in the countryside of the state of São Paulo, Brazil. The experimental analysis highlighted important molecular evidence of a potential new virus from the *Jingmenvirus* group in ticks collected from wild animals. The four pools that were positive included *Amblyomma sculptum* and *A. nodosum* ticks, collected from *Myrmecophaga tridactyla*, *Callithrix penicillata*, and *Cerdocyon thous*. These data suggest that it is a new member of the *Jingmenvirus* group, which we propose to be named Rio Preto tick virus (RPTV). In addition, the RPTV genome was analysed *in silico*, and proteins with high homology to those of the *Jingmenvirus* group were identified. Here, we report the identification of a potentially novel virus found in ticks from wild animals in southeastern Brazil. This study contributes to the epidemiological surveillance of the region and helps to understand the potential risks of the emergence of zoonoses, which can impact human health, in addition to the potential impacts on the fauna.

Keywords: wild animals; emerging virus; ticks; zoonoses; Rio Preto tick virus; *Jingmenvirus*

Introduction

Ticks are obligate hematophagous ectoparasites, which serve as vectors of various infectious agents for domestic and wild animals, and also for humans, who end up being accidental hosts (Dantas-Torres *et al.* 2012, Ogden 2016). Tick-transmitted pathogens to humans are of zoonotic origin, with pathogens maintained in natural cycles involving both domestic and free-roaming animal hosts (Wikel 2018). Tick-borne infections account for a large proportion of vector-borne diseases in many developed and underdeveloped countries and are hence of significant relevance (Rochlin and Toledo 2020).

Jingmenviruses are a new group of viruses transmitted by ticks that were first identified in *Rhipicephalus microplus* ticks collected in the city of Jingmen, Hubei Province, China, in 2010 (Qin *et al.* 2014). According to the International Committee on Taxonomy of Viruses (ICTV), the *Jingmenvirus* group is an unclassified member of the *Flaviviridae* family (Zhang *et al.* 2020). This group is fundamentally different from other members of the family since it consists of segmented single-stranded positive-sense RNA genome (Yu *et al.* 2020) and is composed of four segments. Segment 1 and Segment 3 encode the nonstructural proteins, NSP1 and NSP2, which are genetically and functionally related to the *Orthoflavivirus* NS5 and NS3 proteins, respectively (Wu *et al.* 2023a). In contrast, Segment 2 and Segment 4 are unique to this virus and have, as yet, no known homologues, and likely originated from uncharacterized ancestral viruses (Qin *et al.* 2014, Shi *et al.*

2016). Members of the group includes Jingmen tick virus (JMTV), Mogiana tick virus (MGTV), Alongshan virus (ALSV), Guaico culex virus (GCXV), and Kindia tick virus (KITV) among others (Ladner *et al.* 2016, Kuivanen *et al.* 2019, Wang *et al.* 2019a, Wang *et al.* 2019b, Kartashov *et al.* 2023).

Following the discovery of JMTV in China, it has been encountered in several countries, such as China, Laos PDR, Japan, Turkey, Italy, Kosovo, Romania, Russia, Brazil, Trinidad and Tobago, French Antilles, Colombia, Uganda, Guinea, and Kenya (Qin *et al.* 2014, Ladner *et al.* 2016, Shi *et al.* 2016, Villa Erika *et al.* 2017, Emmerich *et al.* 2018, Souza *et al.* 2018, Sameroff *et al.* 2019, Temmam *et al.* 2019). In addition, a wide range of genetically related viruses have also been reported and are being classified as members of the *Jingmenvirus* group. Other than ticks, viruses from this group were identified in mosquitoes, cattle, sheep, bats, rodents, tortoises, primates, and humans (Colmant *et al.* 2022). In humans, two members of *Jingmenvirus* group, JMTV and ALSV, were implicated in causing disease in humans (Jia *et al.* 2019, Wang *et al.* 2019b). Patients reported an itchy and painful scar at the site of the tick bite, and skin biopsies confirmed viral replication and local inflammation (Jia *et al.* 2019). Retrospective molecular and serological studies found that patients with febrile disease and a history of tick bites were positive for these viruses, including cases suspected of Crimean–Congo haemorrhagic fever (Emmerich *et al.* 2018). Symptoms included lymphadenopathy, headache, fever, and seizures (Jia *et al.* 2019; Wang *et al.* 2019b).

In recent years, many new viruses belonging to the *Flaviviridae* family have been identified using high-throughput sequencing (Zhang *et al.* 2020). Here, we sought to investigate the virome of ticks collected from wild animals using a metagenomic approach, to characterize the viral diversity present in ticks that parasitize wild animals, contributing to the epidemiological surveillance in the region. We report the identification and characterization of the new Rio Preto tick virus (RPTV), a segmented single-stranded positive RNA virus from the *Jingmenvirus* group detected in ticks of the *Amblyomma sculptum* and *A. nodosum* species that were collected from wild animals in Brazil.

Methods

Sample collection

Two hundred seventy-three ticks were collected between August 2018 and December 2021 from wildlife animals sent to the Municipal Zoo of São José do Rio Preto—SP, which is a reference site in the emergency care of wildlife in the region and were collected by the veterinarians who cared for those animals. The ticks were preliminarily identified based on morphological features (Barros-Battesti *et al.* 2006). The identified ticks were separated into 71 pools and stored in cryogenic tubes at −150°C, based on the animal from which they were collected and the tick species. Sex and engorgement status were not considered for separating pools.

Sample preparation

Prior to maceration, ticks were washed thrice with PBS (phosphate-buffered saline) to remove surface impurities. Subsequently, they were macerated with the aid of a pestle, in a 1500 μl microtube, partially on ice, containing Tris-EDTA buffer (TE) (10 mM Tris-HCl, 1 mM ethylenediaminetetraacetic acid (EDTA), pH 7.4) and Proteinase K (20 units/mg). Samples were centrifuged at 12 000 × g for 10 min at 4°C; the supernatant was collected for RNA extraction, which was performed using the Direct-zol RNA MiniPrep kit (Zymo Research, USA) following the manufacturer's instructions.

Species identification through *COI* gene

Subsequently, the ticks were molecularly identified through polymerase chain reaction (PCR), and Sanger sequencing, based on a 710 bp fragment of a region of the mitochondrial gene cytochrome c oxidase subunit I (*COI*) (Folmer *et al.* 1994). Initially, the extracted RNA was converted into complementary DNA (cDNA) using High-Capacity cDNA Reverse Transcription Kit (Applied Biosystems, USA), according to the manufacturer's instructions. The PCR was performed with the Taq DNA Polymerase Recombinant PCR kit (Invitrogen, USA) with a final volume of 25 μl, and the primers used in the reaction were LCO1490 'GGTCAACAAATCATAAAGATATTGG' and HCO2198 'TAAACTTCAGGGTGACCAAAAAATCA' (Folmer *et al.* 1994). Amplification was performed at 94°C for 3 min for initial denaturation to occur, then for 40 cycles at 94°C for 45 s (denaturation), 46°C for 30 s (annealing), and 72°C for 1 min and 10 s (extension), followed by the final extension step at 72°C for 10 min. PCR products were analysed on a 1% agarose gel stained with ethidium bromide. Sequencing was performed using the Sanger technique, using *BigDyeTerminator* v3.1 (Applied Biosystems, USA) and the same primers used for the PCR reaction. Readings were performed in an ABI 3130 XL genetic analyser (Applied Biosystems, USA). The sequences were submitted to the Barcode of Life Data Systems (BOLD Systems) platform, which allows species identification based on the genomic region of interest.

Preparation of genomic libraries and next-generation sequencing

Preparation of genomic RNA sequencing libraries and ribosomal RNA depletion were performed using the Zymo-Seq RiboFree Total RNA Library Kit (Zymo Research, USA). Four RNA libraries were constructed and sequenced. Libraries were prepared using 35 RNA pools. From the 71 RNA pools (Supplementary Table S1), at least 1 pool of each tick species per host was selected. The 35 RNA pools were separated into four libraries (Supplementary Table S1). Validation of libraries was performed by quantification with Qubit dsDNA HS Assay (Invitrogen, USA), and library size was evaluated using High Sensitivity D5000 ScreenTape (Agilent Technologies Inc, USA). Sequencing was performed using the MiSeq platform (Illumina Inc, USA) with 600-cycle V3 cartridges (2 × 300 cycles).

Data analysis

Raw data were demultiplexed and extracted in the fastq format. The reads were treated to remove adapters and library indexes; trimming and filtering were performed using the Genious Prime 2023.0.2 software (https://www.geneious.com). The reads were analysed in RiboDetector software to detect and remove ribosomal RNA sequences (Deng *et al.* 2022). The treated reads were aligned, and the contigs were *de novo* assembled in the SPAdes 3.15.4 software (Bankevich *et al.* 2012). The taxonomic classification of the generated contigs was acquired by Kaiju 1.9.0 (Menzel *et al.* 2016) (https://kaiju.binf.ku.dk/) using complete genome sets available at the National Center for Biotechnology Information (NCBI) (https://www.ncbi.nlm.nih.gov/).

Phylogenetic and genetic distance analysis

The datasets for the phylogenetic and distance analysis were assembled using sequences deposited in GenBank from viral species that display higher similarity based on a Blastx search (https://blast.ncbi.nlm.nih.gov/Blast.cgi) for all four RPTV segments. Sequences were aligned using MAFFT 7 available at https://mafft.cbrc.jp/alignment/servidor/, and the Maximum likelihood phylogenetic trees were built using PhyML 3 (Guindon

and Gascuel 2003) available at the ATGC Montpellier bioinformatics platform (http://www.atgc-montpellier.fr). The substitution model was selected by smart model selection (SMS) (Lefort *et al.* 2017) and branch support by approximate likelihood-ratio test (aLRT) (Anisimova and Gascuel 2006). The phylogenetic trees were edited using the software FigTree v.1.4.4 (Rambaut 2018). The genetic distance was calculated by p-distance using MegaX (Kumar *et al.* 2018). The analysis was based only on the coding region from each fragment.

Rio Preto tick virus molecular detection

The RT-qPCR reaction was performed to confirm the presence of RPTV in tick samples by amplifying a region of the NSP2 protein similar to NS3 located in Segment 3 of the genome. The RT-qPCR reaction was performed with the KiCqStart® One-Step Probe RT-qPCR ReadyMix™ Kit (Sigma, USA) with a final volume of 15 μl; the primers used in the reaction, which amplify a 107 bp fragment, were RPTV_F (AAAGCTCAAGGCATGGCTAC) and RPTV_R (ATGACCAGGAGCTGTTTTGC), and the probe was (FAM-AGTGGCAGTGCTTAGCTGCGTCTTG-BHQ1). The RT-qPCR cycling conditions were 95°C for 3 min and then 40 cycles of 10 s at 95°C and 30 s at 60°C. For a positive sample, the cycle threshold (Ct) value was set at <40, and a plasmid containing the target gene was used as a positive control. All 71 RNA pools were analysed by RT-qPCR.

Virus isolation

The macerate of ticks that were positive for RPTV viral RNA by RT-qPCR was passed through a sterile filter 0.45 μm (Jet Biofil, China), and it was added to baby hamster kidney fibroblast cells (BHK-21; ATCC CCL-10) cultured in Dulbecco's Modified Eagle Medium (DMEM) (Cultilab, Brazil), supplemented with 10% fetal bovine serum (FBS) (Gibco—Thermo Fisher Scientific, USA), and 1000 U/ml penicillin–streptomycin (P/S) (Thermo Scientific, USA). They were cultured in polyethylene bottles 75 cm^2 and maintained in a humidified incubator at 37°C with 5% CO_2 enrichment. For that, 400 μl of the macerate of ticks was inoculated into a monolayer of these cells for 1 h at 37°C. After this step, the inoculum was removed, and DMEM medium was added to the cells, and they were maintained at 37°C with 5% CO_2. The cells were inspected daily until it was possible to observe a cytopathic effect. Next, total RNA was extracted from the supernatant and from the cells using Trizol (Thermo Scientific, USA), according to the manufacturer. The presence of RPTV RNA was assessed by reverse transcription-quantitative polymerase chain reaction (RT-qPCR).

Sanger sequencing

The confirmation of the presence of RPTV in the samples that were RT-qPCR positive for RPTV was done by the Sanger method. To that end, a nested-PCR strategy was used to amplify a region of Segment 3 that had sufficient genetic information to distinguish different representatives from the *Jingmenvirus* group. Briefly, RNA was first converted into cDNA using the High-Capacity cDNA Reverse Transcription Kit (Applied Biosystems, USA), according to the manufacturer's instructions. The PCR reaction was performed with the GoTaq®G2 Green Master Mix (Promega, USA) and the outer primers RPTV_PF 5′-TACGAGCCCAGTGTAGTCCA-3′ and RPTV_PR 5′-CGTACTTCACCCGTTGTGG-3′. Amplification was performed at 95°C for 5 min, then 40 cycles of 94°C for 30 s, 60°C for 1 min, and 72°C for 1 min, followed by the final extension step at 72°C for 5 min. The second reaction was also performed with GoTaq®G2 Green Master Mix (Promega, USA) and the inner primers RPTV_NF 5′-GTCGTCCTCCTGTAATCAAG-3′ and RPTV_NR 5′-CTTGGTGGATCAAGGCTCTA-3′. Amplification was performed at 95°C for 5 min, then 40 cycles of 94°C for 30 s, 58°C for 1 min, and 72°C for 1 min, followed by the final extension step of 72°C for 5 min. The products were analysed on a 1% agarose gel stained with ethidium bromide. Sequencing was performed using *BigDyeTerminator* v3.1 (Applied Biosystems, USA) and the inner primers from the nested-PCR reaction that amplifies a 672 bp fragment. Samples were read on Spectrum Compact CE System equipment (Promega, USA).

Prediction and analysis of three-dimensional protein structures

The nucleotide sequences were translated into amino acids using the Translate Tool (Gasteiger *et al.* 2003) at the ExPASy server, and AlphaFold (Jumper *et al.* 2021) was used to predict the 3D structures of the proteins encoded by the four viral genomic segments. The signal peptides from the structures were deleted using the SignalP—5.0 server (Almagro Armenteros *et al.* 2019), and a Basic Local Alignment Search Tool (BLAST) search was conducted to identify highly homologous structures deposited with the Protein Data Bank (PDB) (https://www.rcsb.org/) for the comparative analysis. The visualization of the superimposition of protein structures and the generation of figures was performed using PyMOL 3D Zalman (Schrodinger 2015).

Results

Tick collection and identification

In total, 273 ticks were collected from 27 hosts, which were initially identified morphologically and separated into 71 pools according to tick species and host. The tick's species identified in this study were *A. sculptum*, being the most prevalent species (68.13%, 186/273), *A. nodosum* (27.47%, 75/273), and *Riphicephalus microplus* (4.40%, 12/273). Information on rescue location, host species, pool ID, number of ticks per pool, and tick species is described in Table S1 of the supplementary material (Fig. 1).

Analysis of the metagenomic data

Illumina sequencing generated a total of 56 177 760 reads (Supplementary Table S2). Genomic sequences from ticks were removed and, after *de novo* assembly, a total of 7 909 059 contigs were classified using the complete genome database by Kaiju, which generated the Krona plots.

The vast majority of contigs, around 5 651 754, were classified as cellular organisms like bacteria and fungi, resulting in 1372 viral contigs. Of all the viral sequences, the most notable was the presence of the complete genome of the JMTV, including all four segments, that appeared in greater scope only in Library 4 (Supplementary Fig. S4), which was composed of ticks of the species *A. sculptum* and *A. nodosum* (information on the generated in the other libraries can be seen in Supplementary Figs. S1, S2 and S3). Of the 35 viral contigs present in Library 4, 10 contigs belong to JMTV. The ticks used in the preparation of Library 4 belonged to the hosts *Myrmecophaga tridactyla* (giant anteater), *Cerdocyon thous* (grab-eating fox), and *Callithrix penicillate* (black-tufted marmoset) (Supplementary Table S1). The sequences from Segments 1, 2, 3, and 4 were deposited on GenBank under the respective accession numbers: PP386533, PP386534, PP386535, and PP386536.

Phylogenetic analysis

The maximum likelihood phylogenetic trees for all four segments were built under the Gly, Thr, and Arg (GTR) + R model, according to SMS selection, based on the nucleotide sequences of the four segments obtained in this study, together with the sequences of the *Jingmenvirus* group previously described (Figs 2–5). For all four

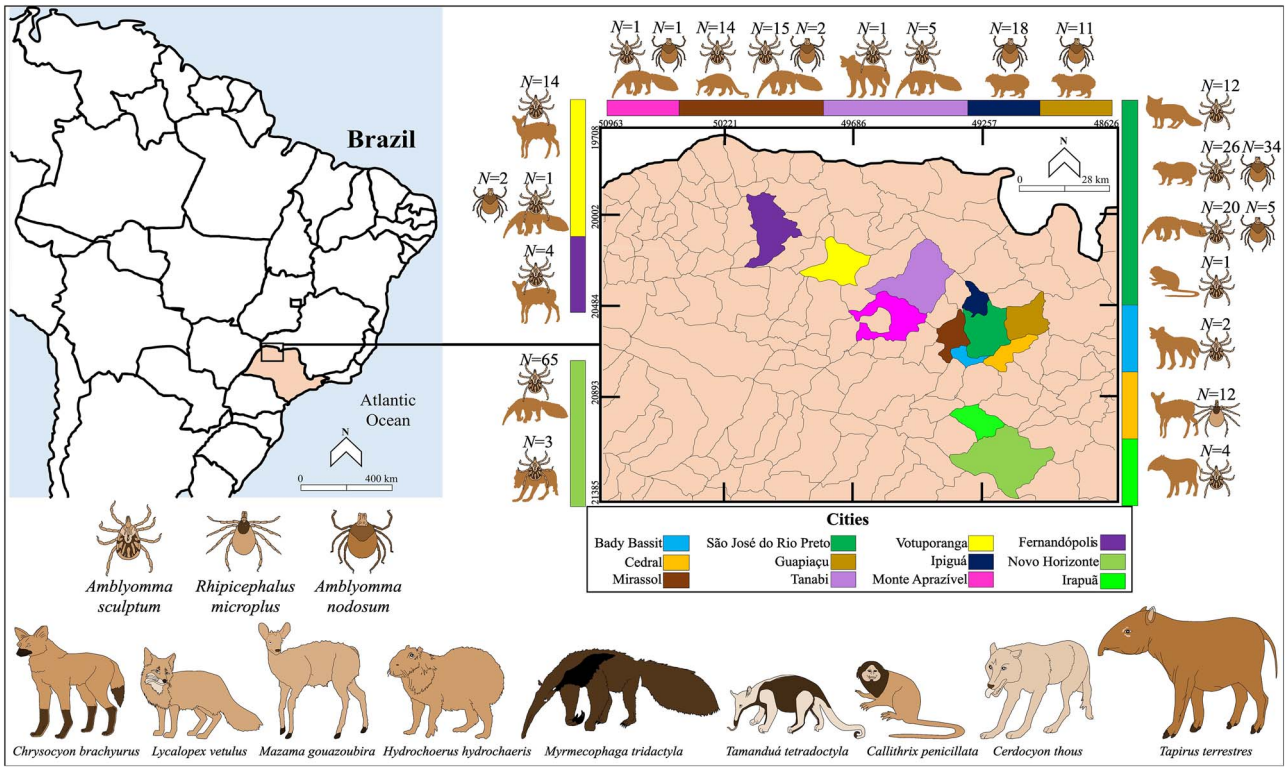

Figure 1. Geographical location from the cities, situated in the northwest region of the state of São Paulo-Brazil, where the wild animals that hosted the ticks analysed in this study were rescued. Wild animals and tick species are represented. 'N' represents the total number of ticks collected per host.

Table 1. Description of the distance between the virus closest to RPTV, for each segment.

	Closest relative (accession number)	Country	p-distance	% of identity
Segment 1	Jingmen tick virus (OP616978.1)	China	0.24918033	75%
Segment 2	Jingmen tick virus (OP616987.1)	China	0.29181338	71%
Segment 3	Jingmen tick virus (MK721571.1)	China	0.25092707	75%
Segment 4	Jingmen tick virus (LC628151.1)	Japan	0.29684601	70%

segments, the virus described in this study lies in a well-supported branch, separately from previously reported JMTVs.

The genetic distance between the closest virus for each fragment is described in Table 1. JMTV, belonging to the Jingmenvirus group, is the closest representative to the virus identified in this study. Distances between all representatives used in the analyses, for all segments, are available in the supplementary material (Supplementary File S1).

Considering the phylogenetic analysis, with a robust separation from other sequences and 25%–30% (all four segments) genetic distance between the closest virus of the group, we suggest that this is a new member of the Jingmenvirus group and we named it Rio Preto tick virus (RPTV).

PCR detection

The 71 tick RNA pools were analysed by RT-qPCR in order to confirm the presence of the RPTV viral genome. Of the 71 pools, four were positive for the presence of RPTV, namely: B79-I collected from a giant anteater; B80-I collected from a black-tufted marmoset; B97-III collected from a giant anteater; and B100-I collected from a crab-eating fox; three pools contained *A. sculptum* ticks and one *A. nodosum*. The positive samples were collected in the cities of São José do Rio Preto and Novo Horizonte. A fragment of Segment 3 from all four samples was amplified by nested PCR and Sanger sequenced. A phylogenetic analysis confirmed RPTV detection in all PCR-positive samples. (Supplementary Fig. S5).

Virus isolation

Tentative virus isolation in BHK-21 cells was performed on all four positive pools. After 48 h, increased cell detachment was observed when compared to the control. The supernatant was used to inoculate fresh BHK-21 cells (second passage). After 48 h, cells and the supernatant were collected. RNA was extracted from the supernatant and cells (except from the first passage of B79-I and B80-I due to availability) from both passages, and RT-qPCR for RPTV was performed. RPTV RNA was detected in the supernatant from the first passage of B79-II, B80I, and B97-III and also in the intracellular content of cells inoculated with B97-III. In the second passage, the RNA was detected only in the intracellular content of cells inoculated with B79-II but not in the supernatant (Fig. 6, Table 2). These results suggest that the BHK-21 cell line is susceptible but probably not permissive to RPTV, since although the virus can be found inside the cell, new virus particles are not being produced. The presence of RPTV RNA in

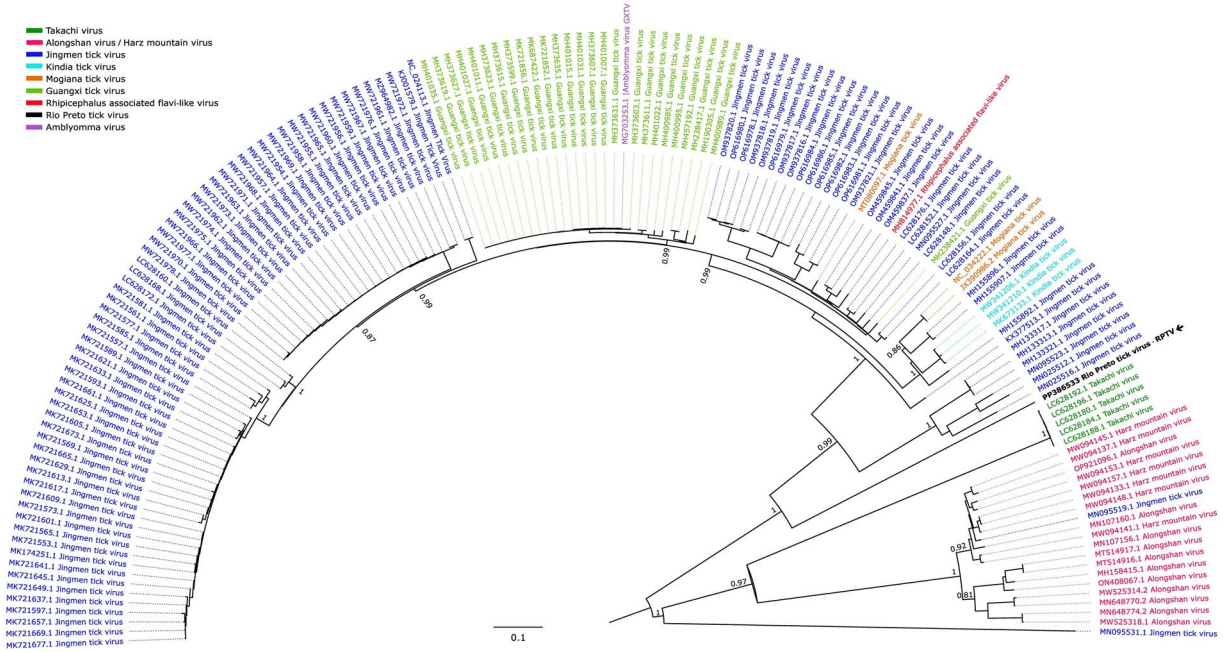

Figure 2. Maximum likelihood phylogenetic tree reconstructed under the GTR + R model based on a dataset of 159 nucleotide sequences of segment 1. The dataset comprises the sequences from this study along with sequences deposited on GenBank from the *Jingmenvirus* group. The virus species are presented according to the classification provided by the sequence authors. Branch support is determined by aLRT, values presented for the main branches when above 0.7.

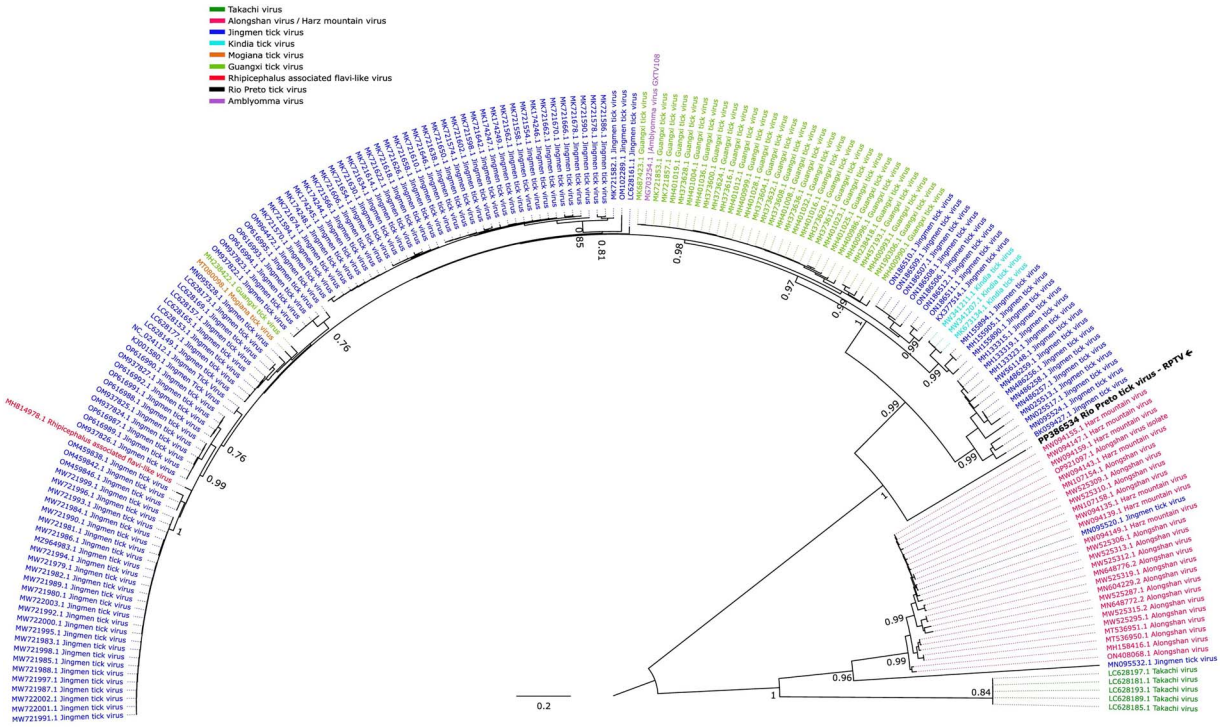

Figure 3. Maximum likelihood phylogenetic tree reconstructed under the GTR + R model based on a dataset of 190 nucleotide sequences of Segment 2. The dataset comprises the sequences from this study along with sequences deposited on GenBank from the *Jingmenvirus* group. The virus species are presented according to the classification provided by the sequence authors. Branch support is determined by aLRT, values presented for the main branches when above 0.7.

the supernatant from Passage 1 can be due to residual virus from the macerate used to inoculate the cells. This also could account for the intracellular content from B79-II Passage 2. In conclusion, viral isolation was not successful and could not be repeated due to sample unavailability.

Genome organization

The RPTV genome described in this work comprises four separate positive-sense linear single-stranded RNA segments, which are called Segments 1, 2, 3 and 4, respectively. In this work, we obtained a genome of 11 789 nucleotides corresponding to

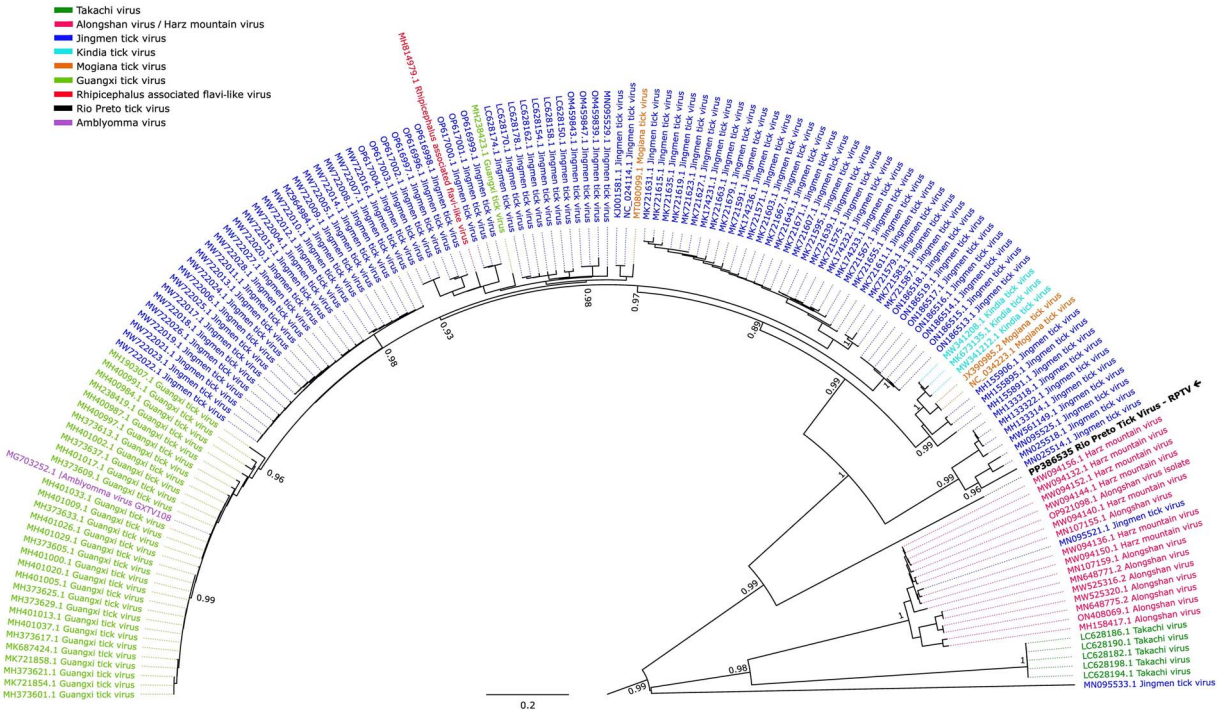

Figure 4. Maximum likelihood phylogenetic tree reconstructed under the GTR + R model based on a dataset of 156 nucleotide sequences of Segment 3. The dataset comprises the sequences from this study along with sequences deposited on GenBank from the *Jingmenvirus* group. The virus species are presented according to the classification provided by the sequence authors. Branch support is determined by aLRT, values presented for the main branches when above 0.7.

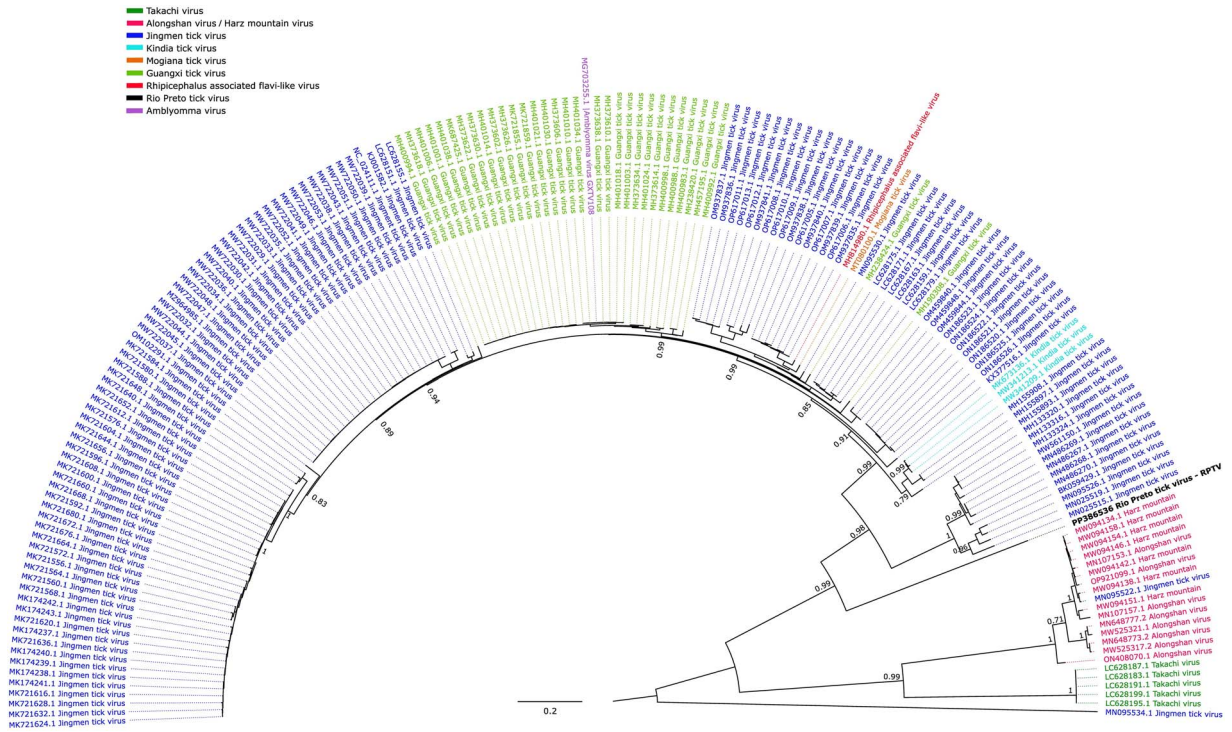

Figure 5. Maximum likelihood phylogenetic tree reconstructed under the GTR + R model based on a dataset of 181 nucleotide sequences of Segment 4. The dataset comprises the sequences from this study along with sequences deposited on GenBank from the *Jingmenvirus* group. The virus species are presented according to the classification provided by the sequence authors. Branch support is determined by aLRT, values presented for the main branches when above 0.7.

Segment 1 (3065 bp), Segment 2 (2981 bp), Segment 3 (2969 bp), and Segment 4 (2774 bp). Segment 1 contains nucleotides encoding the nonstructural protein NSP1, similar to orthoflavivirus NS5 proteins, and was characterized by the conserved RNA-dependent RNA polymerase (RdRp) and methyltransferase (MTase) motifs that are typical of orthoflavivirus. Segment 3 contains nucleotides

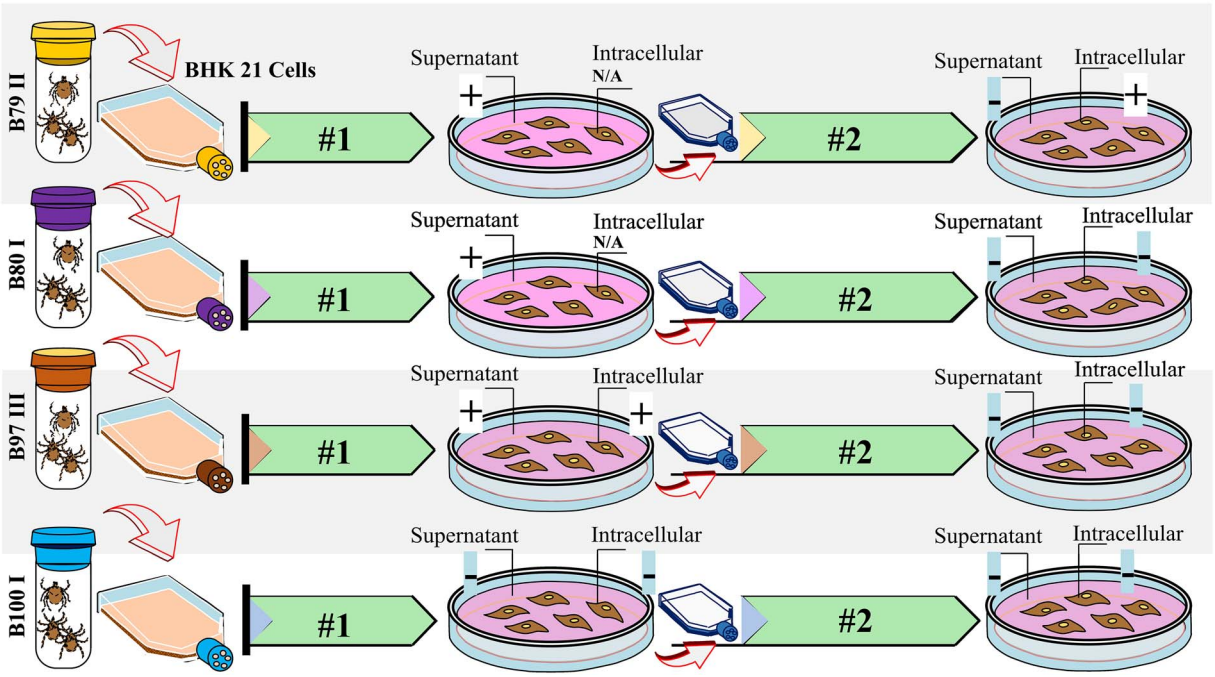

Figure 6. Schematic representation of viral isolation attempts in BHK-21 cells.

Table 2. RT-qPCR Ct values referring to the intracellular and supernatant collected after virus isolation attempts.

	Values Ct RT-qPCR			
	First passage		Second passage	
	Supernatant	Intracellular	Supernatant	Intracellular
B79 II	24.63	N/A	–	30,64
B80 I	25.24	N/A	–	–
B97 III	35.08	36.28	–	–
B100 I	–	–	–	–

N/A: not available. -: negative.

encoding the nonstructural protein NSP2, which also resembles the orthoflavivirus NS2b-NS3 complex. Segment 2 encodes the putative envelope structural protein VP1. Segment 4 has two Open Reading Frame (ORF) that encode the structural proteins VP2 and VP3, which are putative capsid and membrane proteins, respectively (Fig. 7).

Structural analysis

Segment 1: monocistronic RNA that encodes nonstructural NSP1 protein with the conserved motifs for methyltransferase and RNA-dependent RNA polymerase of a typical orthoflavivirus

The structural model of the Segment 1 polyprotein was generated, featuring a signal peptide comprising the first 27 amino acids, followed by an unstructured region, an N-terminal methyltransferase domain (MTase) that is connected by a linker to a C-terminal RNA-dependent RNA polymerase domain (RdRp) (Fig. 8A). This protein is referred to as NSP1 in the *Jingmenvirus* group (Wang *et al.* 2024). The NSP1-RPTV exhibited high structural homology with NS5 from various orthoflaviviruses, including Dengue virus (DENV2) (PDB ID: 5ZQK), Yellow Fever virus (YFV) (PDB ID: 6QSN), Japanese Encephalitis virus (JEV) (PDB ID: 4K6M), Zika virus (ZIKV) (PDB ID: 5TMH), Bovine viral diarrhoea virus (BVDV) (PDB ID: 1S4F), and West Nile virus (WNV) (PDB ID: 2HCN). Comparisons of the MTase (Fig. 9) and RdRp (Fig. 10) domains with orthoflavivirus homologues available in databases confirmed that their overall folds are conserved, as expected. However, specific structural differences were identified that could potentially influence their activities or interactions with drugs or host factors.

The alignment of the linker present in NSP1-RPTV with its corresponding regions in the other orthoflaviviruses (Fig. 8B) indicated that this region in NSP1-RPTV contains a longer insertion, which permits greater flexibility between the MTase and RdRp of RPTV. In addition, the GTR residues are absent from the NSP1-RPTV linker (Fig. 8B), which corresponds to a motif conserved in orthoflavivirus structures, such as DENV, YFV, ZIKV, and JEV (Fig. 8B). GTR motifs play crucial roles in ensuring the structural stability of orthoflavivirus NS5, as they participate in the intricate network of hydrogen bonds spanning both sides of the interface (Ray *et al.* 2006) and have been shown to be essential for the replication of JEV and DENV2 (Züst *et al.* 2011). Interestingly, when comparing the NSP1-RPTV linker with the corresponding region in NSP1 of the JMTV (GenBank ID: BEP27574.1), a similarity was observed in the length of these regions, along with the lack of conservation of the GTR motif (Fig. 8B). This appears to be a common characteristic of NSP1 in viruses belonging to the *Jingmenvirus* group (Liu *et al.* 2024).

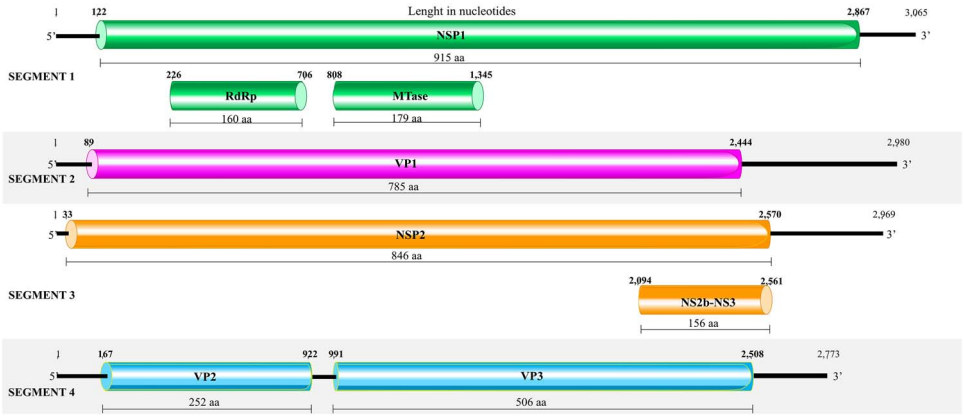

Figure 7. Graphic representation of the four viral genome segments of Rio Preto tick virus (RPTV) showing their ORFs that encode specific proteins, namely: Segment 1 shows the NSP1 nonstructural protein; Segment 2 shows the VP1 envelope structural protein; Segment 3 shows the NSP2 nonstructural protein; and Segment 4 shows the capsid VP2 and membrane VP3 structural proteins.

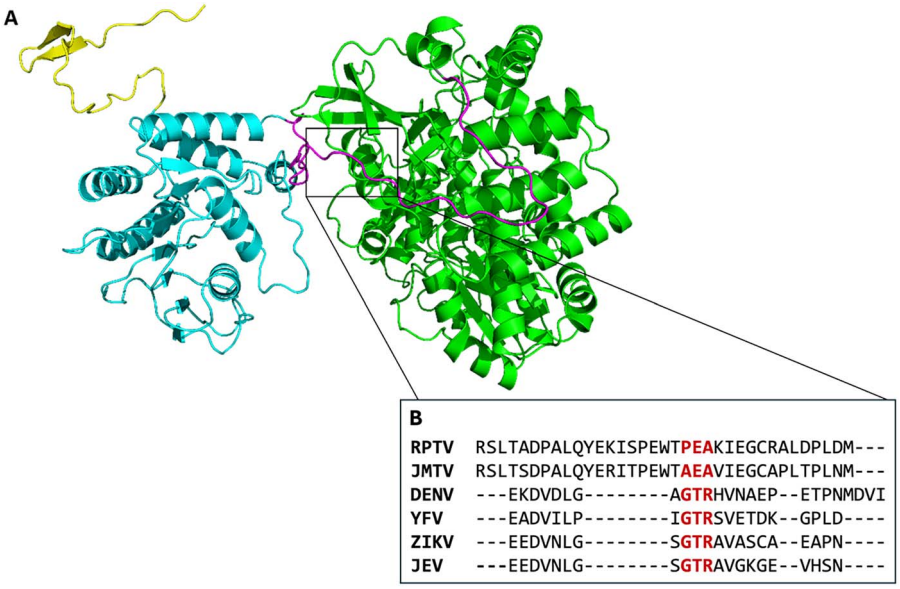

Figure 8. (A) 3D cartoon representation of the full-length NSP1 structure of the RPTV generated by AlphaFold. The model includes the unstructured region (yellow), the methyltransferase domain (cyan), the linker peptide (magenta), and the RNA-dependent RNA polymerase domain (green). (B) Sequence alignment of the linker connecting MTase and RdRP domains of NSP1 in the RPTV virus and its corresponding regions in JMTV, DENV2, ZIKV, JEV, and YFV. The red colour indicates the highly conserved GTR sequence in viruses from the *Flaviviridae* family.

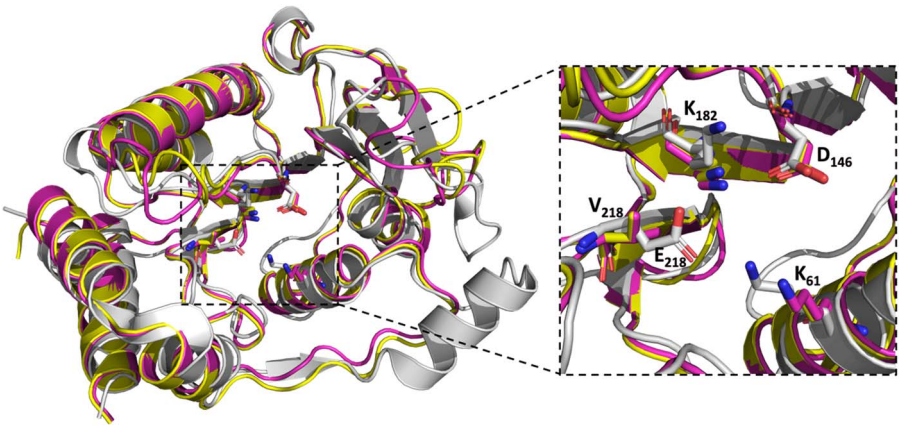

Figure 9. Structural overlap of the 3D models of MTases from RPTV (magenta) and JMTV (GenBank ID: BEP27574.1) (yellow) viruses with the crystallographic structure of the MTase from DENV2 (PDB ID: 5ZQK) (grey). The KDKE catalytic motif in the MTase of DENV2 and the corresponding KDKV catalytic residues in the MTases of RPTV and JMTV are shown as sticks.

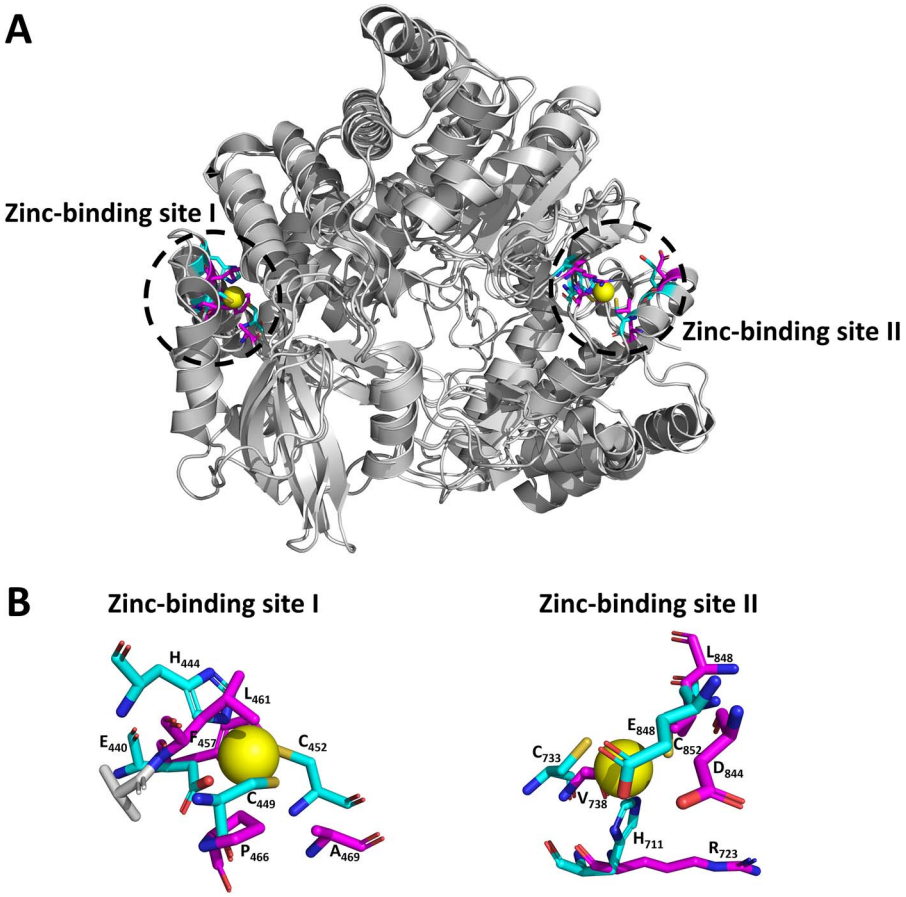

Figure 10. (A) Structural overlap of the 3D model of RdRp from RPTV with the crystallographic structure of RdRp from DENV2 (PDB ID: 5ZQK). The residues belonging to zinc-binding sites I and II in DENV2-RdRp (cyan) and their corresponding residues in RPTV-RdRp (magenta) are highlighted. (B) Overlap of the amino acids from zinc-binding sites I and II of DENV2-RdRp with their corresponding residues in RPTV RdRp. Yellow spheres represent the zinc ion.

Methyltransferase

The entire K_{61}-D_{146}-K_{181}-E_{217} (Dengue virus MTase numbering) motif, essential for 2′-O methylation, is not fully conserved in RPTV (Fig. 9). Viral methyltransferases possess a K-D-K-E motif, which is involved in the enzymatic transfer of a methyl group to the cap-acceptor site of the RNA strand (Ramdhan and Li 2022). Moreover, this motif forms the active site of the 2′-O MTases of Vaccinia virus VP39 (Schnierle *et al.* 1994). The K-D-K-E tetrad is conserved in various MTases of orthoflaviviruses (Ramdhan and Li 2022), except for the MTase from YF, which carries an E_{217}Q mutation. However, this substitution is presumed to induce only a minor stereochemical alteration, as these residues are structurally similar despite the change in charge from negative to neutral.

In contrast, in the MTase of RPTV described here (Fig. 9), the extended, negatively charged side chain of glutamic acid (E_{217}) is drastically replaced by the short, uncharged, and hydrophobic side chain of valine (V_{217}). This same point substitution was observed in the MTase of JMTV (GenBank ID: BEP27574.1) (Fig. 9), a virus that, like RPTV, belongs to the *Jingmenvirus* group. In other words, this feature appears to be characteristic of the MTases of viruses within this group.

The role of E_{217} remains unclear, but this residue is thought to significantly influence the conformation of the RNA-binding pocket (Wang *et al.* 2024). The E_{217}V mutation alters the cavity formed by this motif, giving it distinct biochemical properties compared to other methyltransferases, including MTase-YF with the E_{217}Q mutation. To further investigate these structural changes, the ProteinPlus server (Schnierle *et al.* 1994) was used to analyse the MTase enzyme cavity. As shown in Table 3, the E_{217}V substitution modifies the volume, surface, and depth of the enzyme's binding pocket.

Table 3. Properties of the cavity formed by the catalytic residues K-D-K-V of RPTV compared to the cavity of the K-D-K-E motif normally encountered in orthoflaviviruses. The molecular properties were calculated using the ProteinPlus server (Anisimova and Gascuel 2006).

Motif	K-D-K-E	K-D-K-V
Volume	281.86 A^3	285.82 A^3
Surface area	569.42 A^2	529.1 A^2
Channel depth	10.5 Å	12.56 Å

RNA-dependent RNA polymerase

The structural analysis of the RNA-dependent RNA polymerase (RdRp) of RPTV indicates that this enzyme, like the RdRp from hepatitis C virus (HCV) (PDB ID: 4WTG) and from classical swine fever virus (CSFV) (PDB ID: 1SF4), does not possess the ion binding sites identified in homologous orthoflavivirus enzymes (Fig. 10A). In contrast, at positions E_{440}, H_{444}, C_{449}, and C_{452} (DENV structure

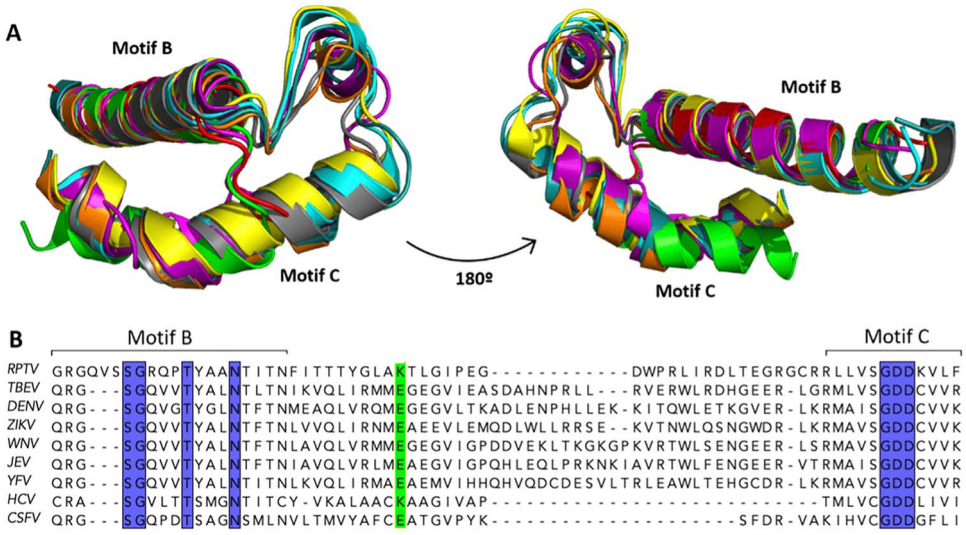

Figure 11. (A) Structural comparison of Motif B, Motif C and the region between B-C of the RPTV virus RdRp protein (green) and these regions in the RdRp proteins of other orthoflaviviruses: TBEV (purple), DENV (grey), ZIKV (orange), WNV (deep teal), JEV (cyan), YFV (yellow), HCV (red), and CSFV (magenta). (B) Sequence alignment of Motif B, Motif C, and the region between B-C of the RdRp of RPTV and the corresponding regions in the same proteins of the orthoflaviviruses analysed in the structural alignment. The blue colour represents the highly conserved active site residues, and the green colour represents the amino acid K_{641} in the RdRp of RPTV and the equivalent residues in the other RdRp of orthoflaviviruses.

numbering), which define the first zinc-binding site, the RPTV virus has the corresponding residues F_{457}, L_{461}, P_{466}, and A_{469} (RPTV structure numbering) (Fig. 10B and Fig. S6, Supplementary Material). Additionally, in the second zinc-binding site, composed of residues H_{711}, C_{733}, E_{848}, and C_{852}, which are conserved in DENV (PDB ID: 5ZQK), JEV (PDB ID: 4K6M), ZIKV (PDB ID: 5WZ3), and WNV (PDB ID: 2HCN), the residues R_{723}, V_{738}, D_{844}, and L_{848} (RPTV structure numbering) are found in RPTV (Fig. 10B and Fig. S6, Supplementary Material). These substitutions result in conformational and charge changes in these regions, potentially leading to a lack of specificity for the Zn^{2+} ion in the RdRp of this newly discovered virus.

Host specificity and residues between RNA-dependent RNA polymerase catalytic motifs B and C of RdRp

Yang *et al.* (2021) determined that the residues between the RdRp catalytic motifs B and C possess host-related diversity, and host adaptation-related factors have driven changes in this region, which may serve to indicate whether it belongs to a tick-borne, mosquito-borne, vertebrate-specific, or insect-specific orthoflavivirus (Yang *et al.* 2021). Structural analysis and comparisons with the corresponding regions of RdRp structures of viruses from different hosts possess two helices connected by a loop, except in HCV RdRp, which lacks the helix in this region (Fig. 11A). The aforementioned region of RPTV, as well as the same region in HCV and CSFV, has the shortest loops when compared to the other RdRps of the viruses analysed (Fig. 11A), but just the RdRp of the RPTV and HCV virus are characterized by the presence of a positively charged, solvent accessible K_{641} residue in a position where the negatively charged E is conserved in other orthoflaviviruses from diverse hosts (Fig. 11B and Supplementary Figs. S7, S8). Interestingly, this anomaly is not observed in the RdRps of other viruses belonging to the *Jingmenvirus* group, which also share high identity with RPTV (Fig. S7, Supplementary Material). In viruses such as JMTV, ALSV, and Yanggou tick virus (YGTV), the K_{641} residue is replaced by V_{641} or R_{641} (Fig. S7, Supplementary Material). Furthermore, primary alignment of the amino acid residues in motifs B and C of RPTV with the equivalent regions in other orthoflavivirus RdRps shows that the active site is conserved (Fig. 11B).

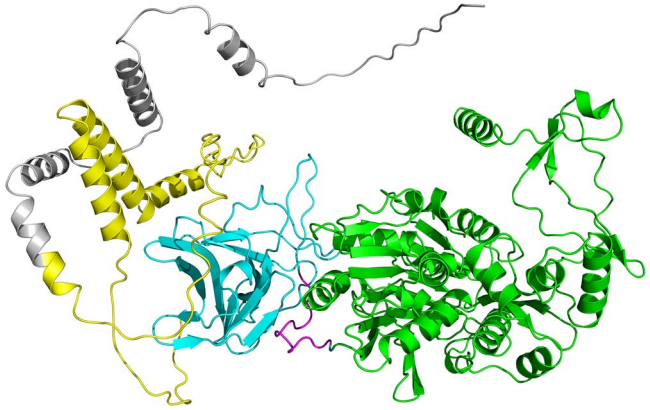

Figure 12. Structural cartoon model of the full-length NSP2 of the RPTV obtained by AlphaFold. The model includes the unstructured region (grey), the transmembrane protein domain (yellow), the serine protease domain (cyan), the linker peptide (magenta), and the helicase domain (green).

Segment 3: monocistronic RNA that encodes nonstructural NSP2 protein with the conserved motifs for protease and helicase of a typical orthoflavivirus

The structural model of the polyprotein of Segment 3 consists of a 58 amino acid signal peptide, followed by a transmembrane protein, and an N-terminal serine protease domain ($NSP2_{PRO}$) that is connected by a linker peptide to a C-terminal helicase ($NSP2_{HE}$) (Fig. 12).

Based on root-mean-square deviation (RMSD) values of atomic positions (Table 4), the model structure of the $NSP2_{PRO}$-RPTV exhibited significant structural homology with the proteases from orthoflavivirus, including DENV, Murray Valley Encephalitis Virus (MVEV), YFV, and HCV (Fig. 13), and among these, the $NSP2_{PRO}$ from MVEV showed the greatest structural homology with

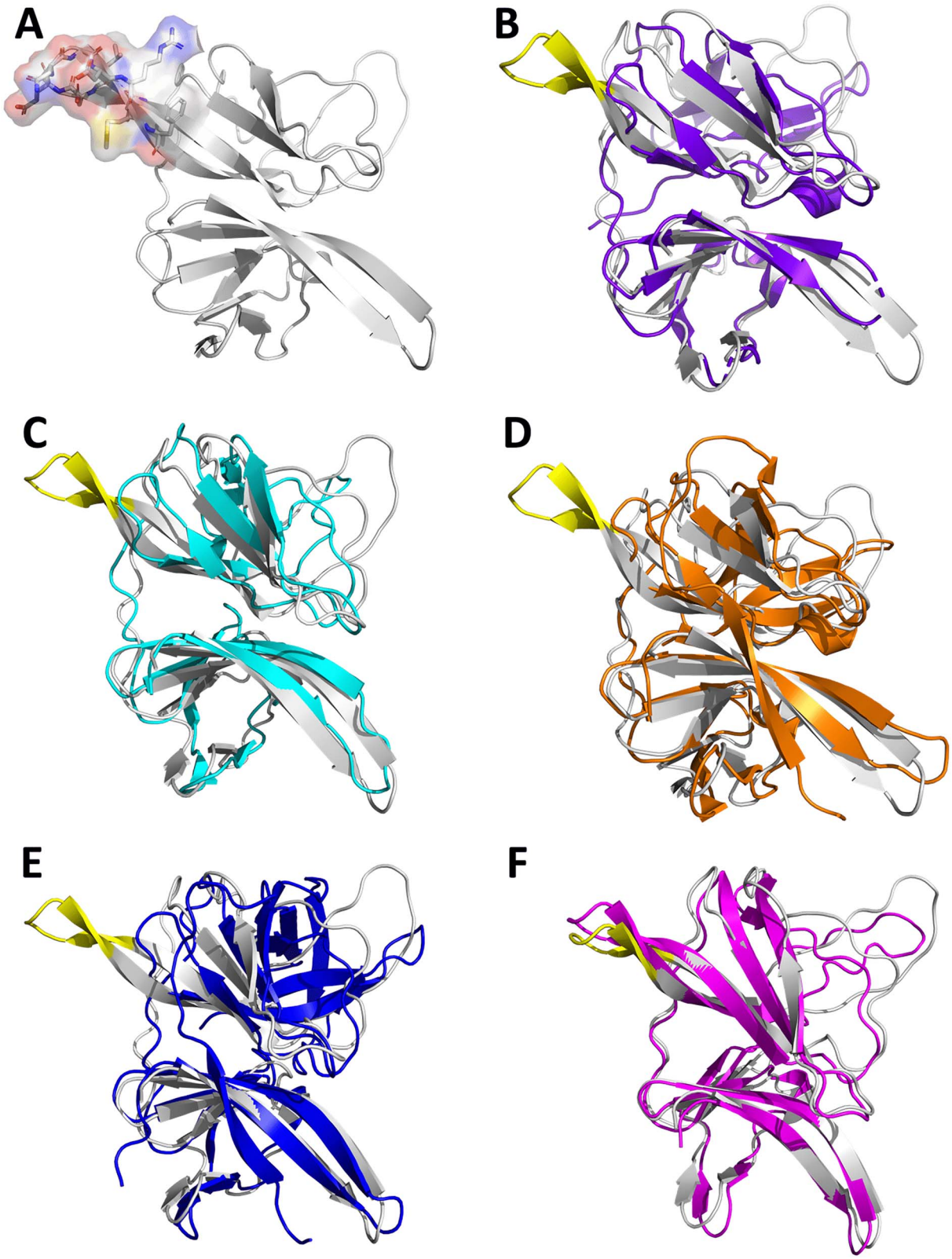

Figure 13. Structural cartoon model of $NSP2_{PRO}$ of the RPTV, highlighting in sticks the amino acid residues belonging to the β-$sheet_{328–335}$ domain (A). Overlay of the 3D model of $NSP2_{PRO}$-RPTV with the $NS3_{PRO}/NSP2_{PRO}$ of DENV (B), MVEV (C), ZIKV (D), YFV (E), and JMTV (F). The β-$sheet_{328–335}$ domain of $NSP2_{PRO}$-RPTV is highlighted in yellow.

$NSP2_{PRO}$-RPTV (Table 4). However, although a broad structural similarity has been identified, an elongated β-$sheet_{328–335}$ domain—~12 Å—amphipathic and exposed to solvent (Fig. 13A) differentiates $NSP2_{PRO}$-RPTV from other orthoflavivirus $NS3_{PRO}$, which have a random coil in this region (Fig. 13B–E). This same β-sheet domain of $NSP2_{PRO}$-RPTV was also observed in the structural model of $NSP2_{PRO}$ from the JMTV species (GenBank ID: QHT72481.1) (Fig. 13F), and maintenance of this region

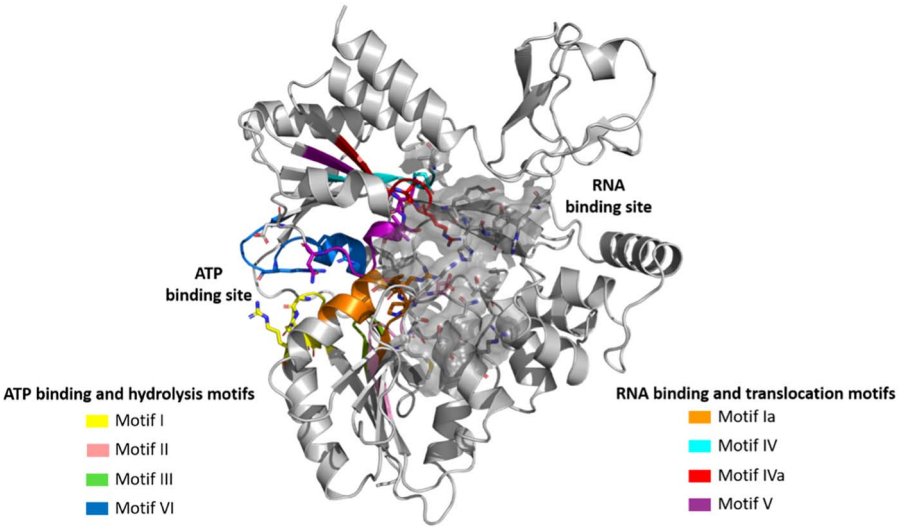

Figure 14. Helicase of NSP2 of RPTV presented in different colours, highly conserved motifs in viral/DEAH-like subfamilies. ATP binding site and RNA binding site residues are represented in sticks. The RNA interaction surface of the helicase was added.

Table 4. RMSD values between the 3D model of the $NSP2_{PRO}$-RPTV and the other $NS3_{PRO}/NSP2_{PRO}$ deposited in the PDB or GenBank.

Virus	PDB or GenBank code	RMSD (Å)
DENV	2VBC	5.286
MVEV	2WV9	2.209
YFV	6URV	2.446
ZIKV	7VXX	2.324
JMTV	QHT72481.1	1.660

ensured high structural homology between these proteases (Table 4).

The model structure of $NSP2_{HE}$ exhibited structural homology with protein structures of the helicase from ALSV (PDB ID: 6 M40), TBEV (PDB ID: 7JNO), BVDV (PDB ID: 5GVU), and CSFV (PDB ID: 4CBH). The analysis of $NSP2_{HE}$-RPTV indicated structural homology with enzymes from orthoflavivirus deposited in the databases, such that the eight main motifs, adenosine triphosphate (ATP) binding site, and RNA binding site exhibit conserved characteristics of *Flaviviridae* family (Fig. 14).

Segment 2 is monocistronic RNA that encodes structural VP1, and Segment 4 is a bicistronic RNA that encodes structural VP2 and VP3

The structural model of a polyprotein corresponding to Segment 1 was generated and consists of VP1 flanked by N- and C-terminal transmembrane regions. The structural model of a polyprotein was generated using Segment 4, which contains an N-terminal VP2 and VP3 encoded by overlapping ORFs within this segment. The BLAST search encountered no significant similarity with structures deposited with databases, making it impossible to perform a detailed comparative structural analysis of these proteins.

Discussion

In this study, we discovered a virus related to the *Jingmenvirus* group in *A. nodosum* and *A. sculptum* ticks collected from three distinct wild animal species: the giant anteater, black-tufted marmoset, and crab-eating fox. The phylogenetic analysis revealed that the sequence from this virus grouped separately from all other members of the group, with strong branch support. In addition, the genetic distance data showed a 25%–30% distance from the closest virus. Altogether, these findings strongly suggest that this is a new virus, which we have named Rio Preto tick virus (RPTV) after the region where it was discovered.

The structural evaluation of the 3D model of the protein encoded by RPTV Segment 1, which is related to the NS5 protein from orthoflavivirus, allowed the identification of regions with significant structural differences. Segment 1 encodes the NSP1 protein, which consists of an MTase and an RdRp (Wang *et al.* 2024). The major difference between NSP1-RPTV and other NS5 proteins from the *Flaviviridae* family is the absence of the GTR motif in the linker connecting the MTase and RdRp domains. The absence of this motif appears to be a characteristic of viruses in the *Jingmenvirus* group (Liu *et al.* 2024). In addition, the K_{61}-D_{146}-K_{182}-E_{218} motif, which belongs to the MTase, is also not fully conserved in RPTV, as E_{217} is replaced by V_{217}. This same substitution was observed in the JMTV species, which also belongs to the *Jingmenvirus* group.

The entire K_{61}-D_{146}-K_{181}-E_{217} motif is essential for 2′-O methylation, whereas N-7 methylation requires only D (Ray *et al.* 2006). Studies have revealed that 2′-O methylation of the mRNA 5′ cap in these viruses is important for evasion from the host innate immune responses (Züst *et al.* 2011, Szretter *et al.* 2012); thus, RNA modifications, such as 2′-O-methylation, provide a molecular signature for the host defence system to discriminate between self and nonself mRNA (Züst *et al.* 2011). However, 2′-O methyltransferase activity has been demonstrated to be absent in several paramyxoviruses, such as the Newcastle disease virus (NDV) and respiratory syncytial virus (RSV) (Colonno and Stone 1976, Barik 1993). Studies investigating host defence against an orthoflavivirus lacking 2′-O MTase activity have shown that interferon-induced protein with tetratricopeptide repeats 1 (IFIT1) selectively interacts with 5′-capped mRNA lacking 2′-O methylation, leading to the inhibition of its translation. Thus, IFIT1 participates in antiviral responses that target 5′-capped mRNA lacking 2′-O methylation and a valine-to-glutamic acid mutation in MTase of RPTV could increase the ability of its viral RNA to shield itself from interferon attack in potential new hosts, suggesting that the absence of the entire tetrad may be relevant for host specificity.

Despite sequence differences, the fundamental structural characteristics of RdRps are conserved in RPTV, likely due to their essential role in genome replication and transcription. However, the structural homology between the RdRp-RPTV and the RdRp-JMTV suggests that similar to JMTV RdRp, RPTV RdRp may require MTase for an optimal transition from initiation to elongation—unlike what is observed for the MTases of viruses in the *Flaviviridae* family (Wang *et al.* 2024). In general, even with the advances in structural analysis, it should be emphasized that the ideal would be to obtain 3D structures by experimental methods, increasing the accuracy of the results presented.

In Brazil, so far, there have been no serological studies to determine if viruses from the *Jingmenvirus* group are circulating in humans and causing disease. Four studies reported viruses from the group, though some of them were first referred to as Mogiana tick virus (MGTV), they are now all considered JMTV (Maruyama *et al.* 2014, Villa Erika *et al.* 2017, Souza *et al.* 2018, Pascoal *et al.* 2019). The viruses were found in cattle or *R. microplus* tick, a parasite of these animals. The new RPTV identified in this study was found in *A. nodosum* and *A. sculptum* ticks. Although JMTV was detected in other species of the *Amblyomma* genus, this is the first report of a member of the group in these species, which are known to parasite wild animals' (Martins *et al.* 2017). The ticks in which RPTV was detected were parasitizing wild free-living mammals from three different species. They were rescued in two different cities: São José do Rio Preto and Novo Horizonte, which are not directly adjacent, being 85 km apart. This suggests that RPTV is circulating in the northwest region of the state of São Paulo. Unfortunately, due to sample unavailability, we were unable to confirm if the wild animals from which the ticks were removed were also infected by the virus, and therefore, we cannot confirm if these species serve as vertebrate hosts of RPTV, participating in a potential arbovirus cycle.

Although it has not been experimentally proven, there is increasing evidence that Jingmenviruses are arboviruses, cycling between arthropod and invertebrate hosts (Colmant *et al.* 2022). Genetic evidence includes the codon usage bias that is consistent with dual host cycling and the phylogenetic data that show the distance between clades to be more influenced by geographic distance than by host species (Maruyama *et al.* 2014, Guo *et al.* 2020). Moreover, naturally and experimentally infected ticks showed accumulation of virus in the salivary glands that could be transmitted through the bite and ticks that were detached from infected patients also tested positive (Jia *et al.* 2019). Unfortunately, in our study, we were unable to isolate RPTV, a limitation also reported by others, and therefore, further biological and functional studies could not be made (Wu *et al.* 2023b).

Given the broad spectrum of vertebrate and tick hosts, the global distribution of Jingmenviruses, the rising number of virus detections within this group, and their known association with febrile illnesses in humans, Jingmenviruses represent a significant potential threat to public health, with potential risk of zoonotic emergence, that should be deeply studied and surveilled.

In this study, we identify a novel member of the *Jingmenvirus* group, named Rio Preto tick virus (RPTV), circulating in ticks from wild animals in the northwest region of São Paulo state. Additional research is needed to understand its host range and assess its pathogenic potential in animals and humans.

Acknowledgements

This work was carried out as a master's thesis of DBG (Programa de Pós-graduação em Microbiologia, UNESP) and was supported by the following grants: D.B.G. thanks the Coordenação de Aperfeiçoamento de Pessoal de Nível Superior-Brasil (CAPES, process number: 88887.607716/2021-00). D.B.G. thanks FAPESP (process numbers: 2023/04491-0). C.B. was financially supported by a PNPD-CAPES scholarship—Coordenação de Aperfeiçoamento de Pessoal de Nível Superior (Finance Code 001). V.G.d.C. and R.B.M. were supported by an UNESP Post-doctoral scholarship, with project n. 4320 and n. 4339 (Edital PROPe 13/2022, Nov 22–July 2023). V.G.d.C. also received a CNPq/FAPESP Post-doctoral scholarship process n. 151207/2023-2, 2023/10809-3). P.R. thanks the Fapergs n° 23/2551-000222-4, CNPq n° 405786/2022-0 and FAPESP (process number: 2021/00603-3 and 2023/01598-9). R.K.A. thanks CNPq n° 309940/2019-2 and FAPESP (process number: 2020/08615-8). C.G. thanks FAPESP (process numbers: 2020/13921-0; 2022/10941-6 and 2024/00876-8). A.C.L. thanks CNPq Proc. no.316575/2021-6. M.L.N. is funded by a research grant from FAPESP (Fundação de Amparo à Pesquisa do Estado de São Paulo—Grant 2022/03645-1), and by the Centers for Research in Emerging Infectious Diseases (CREID), 'The Coordinating Research on Emerging Arboviral Threats Encompassing the Neotropics (CREATE-NEO)' grant U01AI151807. This work is also supported by INCT Viral Genomic Surveillance and One Health by CNPq grant 4057586/2022-0. M.L.N. is a CNPq Research Fellow. J.P.A.J. thanks Fapergs n° 23/2551-000222-4 and CNPq n° 405786/2022-0.

Supplementary data

Supplementary data are available at *VEVOLU Journal* online.

Conflict of interest: None declared.

Funding

None declared.

Data availability

Data deposition: The sequences reported in this paper have been deposited in the GenBank database (accession nos. PP386533, PP386534, PP386535, PP386536). The Sequence Read Archive (SRA) is available for consultation (accession numbers SAMN40000145, SAMN40000146, SAMN40000147, SAMN40000148).

References

Almagro Armenteros JJ, Tsirigos KD, Sønderby CK *et al.* SignalP 5.0 improves signal peptide predictions using deep neural networks. *Nat Biotechnol* 2019;**37**:420–3. https://doi.org/10.1038/s41587-019-0036-z

Anisimova M, Gascuel O. Approximate likelihood-ratio test for branches: a fast, accurate, and powerful alternative. *Syst Biol* 2006;**55**:539–52. https://doi.org/10.1080/10635150600755453

Bankevich A, Nurk S, Antipov D *et al.* SPAdes: a new genome assembly algorithm and its applications to single-cell sequencing. *J Comput Biol* 2012;**19**:455–77. https://doi.org/10.1089/cmb.2012.0021

Barik S. The structure of the 5′ terminal cap of the respiratory syncytial virus mRNA. *J Gen Virol* 1993;**74**:485–90. https://doi.org/10.1099/0022-1317-74-3-485

Barros-Battesti DM, Arzua M, Bechara GH. *Carrapatos de importância médico-veterinária da região Neotropical: Um Guia Ilustrado Para identificação de espécies. São Paulo, ICTTD-3*-Instituto Butantan, 2006.

Colmant AMG, Charrel RN, Coutard B. Jingmenviruses: Ubiquitous, understudied, segmented flavi-like viruses. *Front Microbiol* 2022;**13**:997058. https://doi.org/10.3389/fmicb.2022.997058

Colonno RJ, Stone HO. Newcastle disease virus mRNA lacks 2′-O-methylated nucleotides. *Nature* 1976;**261**:611–4. https://doi.org/10.1038/261611a0

Dantas-Torres F, Chomel BB, Otranto D. Ticks and tick-borne diseases: a one health perspective. *Trends Parasitol* 2012;**28**:437–46. https://doi.org/10.1016/j.pt.2012.07.003

Deng Z-L, Münch PC, Mreches R *et al.* Rapid and accurate identification of ribosomal RNA sequences via deep learning. *Nucleic Acids Res* 2022;**50**:e60–0. https://doi.org/10.1093/nar/gkac112

Emmerich P, Jakupi X, von Possel R *et al.* Genetics, evolution: viral metagenomics, genetic and evolutionary characteristics of Crimean-Congo hemorrhagic fever orthonairovirus in humans, Kosovo. *Infect Genet Evol* 2018;**65**:6–11. https://doi.org/10.1016/j.meegid.2018.07.010

Folmer O, Black M, Wr H *et al.* DNA primers for amplification of mitochondrial cytochrome C oxidase subunit I from diverse metazoan invertebrates. *Mol Mar Biol Biotechnol* 1994;**3**:294–9.

Gasteiger E, Gattiker A, Hoogland C *et al.* ExPASy: the proteomics server for in-depth protein knowledge and analysis. *Nucleic Acids Res* 2003;**31**:3784–8. https://doi.org/10.1093/nar/gkg563

Guindon S, Gascuel O. A simple, fast, and accurate algorithm to estimate large phylogenies by maximum likelihood. *Syst Biol* 2003;**52**:696–704. https://doi.org/10.1080/10635150390235520

Guo J-J, Lin X-D, Chen Y-M *et al.* Diversity and circulation of Jingmen tick virus in ticks and mammals. *Virus Evol* 2020;**6**:veaa051. https://doi.org/10.1093/ve/veaa051

Jia N, Liu H-B, Ni X-B *et al.* Emergence of human infection with Jingmen tick virus in China: a retrospective study. *EBioMedicine* 2019;**43**:317–24. https://doi.org/10.1016/j.ebiom.2019.04.004

Jumper J, Evans R, Pritzel A *et al.* Highly accurate protein structure prediction with AlphaFold. *Nature* 2021;**596**:583–9. https://doi.org/10.1038/s41586-021-03819-2

Kartashov MY, Gladysheva AV, Naidenova EV *et al.* Molecular and genetic characteristics of the multicomponent flavi-like Kindia tick virus (Flaviviridae) found in ixodes ticks on the territory of the Republic of Guinea. *Vopr Virusol* 2023;**67**:487–95. https://doi.org/10.36233/0507-4088-145

Kuivanen S, Levanov L, Kareinen L *et al.* Detection of novel tick-borne pathogen, Alongshan virus, in Ixodes ricinus ticks, southeastern Finland, 2019. *Euro Surveill* 2019;**24**:1900394. https://doi.org/10.2807/1560-7917.ES.2019.24.27.1900394

Kumar S, Stecher G, Li M *et al.* MEGA X: molecular evolutionary genetics analysis across computing platforms. *Mol Biol Evol* 2018;**35**:1547–9. https://doi.org/10.1093/molbev/msy096

Ladner JT, Wiley MR, Beitzel B *et al.* A multicomponent animal virus isolated from mosquitoes. *Cell Host Microbe* 2016;**20**:357–67. https://doi.org/10.1016/j.chom.2016.07.011

Lefort V, Longueville JE, Gascuel O. SMS: smart model selection in PhyML. *Mol Biol Evol* 2017;**34**:2422–4. https://doi.org/10.1093/molbev/msx149

Liu Z, Peng Q, Han P *et al.* Crystal structures of RNA-dependent RNA polymerases from Jingmen tick virus and Alongshan virus. *hLife* 2024;**2**:18–31. https://doi.org/10.1016/j.hlife.2023.10.006

Martins T, Igayara-Souza C, Sanches T *et al.* Diversidade de carrapatos (Acari: Ixodidae) em animais silvestres recebidos pelo Zoológico municipal de Guarulhos. *Ars Vet* 2017;**33**:20–5. https://doi.org/10.15361/2175-0106.2017v33n1p20-25

Maruyama SR, Castro-Jorge LA, Ribeiro JMC *et al.* Characterisation of divergent flavivirus NS3 and NS5 protein sequences detected in Rhipicephalus microplus ticks from Brazil. *Mem Inst Oswaldo Cruz* 2014;**109**:38–50. https://doi.org/10.1590/0074-0276130166

Menzel P, Ng KL, Krogh A. Fast and sensitive taxonomic classification for metagenomics with kaiju. *Nat Commun* 2016;**7**:11257. https://doi.org/10.1038/ncomms11257

Ogden NH. Lindsay LR. Effects of climate and climate change on vectors and vector-borne diseases: ticks are different. *Trends in Parasitology* 2016;**32**:646–56.

Pascoal JO, Siqueira SM, Maia RC *et al.* Detection and molecular characterization of Mogiana tick virus (MGTV) in Rhipicephalus microplus collected from cattle in a savannah area, Uberlândia, Brazil. *Ticks Tick Borne Dis* 2019;**10**:162–5. https://doi.org/10.1016/j.ttbdis.2018.10.002

Qin X-C, Shi M, Tian J-H *et al.* A tick-borne segmented RNA virus contains genome segments derived from unsegmented viral ancestors. *Proc Natl Acad Sci* 2014;**111**:6744–9. https://doi.org/10.1073/pnas.1324194111

Rambaut A. Figtree v1.4.4. Institute of Evolutionary Biology, University of Edinburgh, Edinburgh, 2018.

Ramdhan P, Li C. Targeting viral Methyltransferases: an approach to antiviral treatment for ssRNA viruses. *Viruses* 2022;**14**:379. https://doi.org/10.3390/v14020379

Ray D, Shah A, Tilgner M *et al.* West Nile virus 5′-cap structure is formed by sequential guanine N-7 and ribose 2′-O methylations by nonstructural protein 5. *J Virol* 2006;**80**:8362–70. https://doi.org/10.1128/JVI.00814-06

Rochlin I, Toledo A. Emerging tick-borne pathogens of public health importance: a mini-review. *J Med Microbiol* 2020;**69**:781–91. https://doi.org/10.1099/jmm.0.001206

Sameroff S, Tokarz R, Charles RA *et al.* Viral diversity of tick species parasitizing cattle and dogs in Trinidad and Tobago. *Sci Rep* 2019;**9**:1–10. https://doi.org/10.1038/s41598-019-46914-1

Schnierle BS, Gershon PD, Moss B. Mutational analysis of a multifunctional protein, with mRNA 5′ cap-specific (nucleoside-2′-O-)-methyltransferase and 3′-adenylyltransferase stimulatory activities, encoded by vaccinia virus. *J Biol Chem* 1994;**269**:20700–6. https://doi.org/10.1016/S0021-9258(17)32049-5

Schrodinger LJV. The PyMOL molecular graphics system. *Version* 2015;**1**:8.

Shi M, Lin X-D, Vasilakis N *et al.* Divergent viruses discovered in arthropods and vertebrates revise the evolutionary history of the Flaviviridae and related viruses. *J Virol* 2016;**90**:659–69. https://doi.org/10.1128/JVI.02036-15

Souza WM, Fumagalli MJ, Torres Carrasco AO *et al.* Viral diversity of Rhipicephalus microplus parasitizing cattle in southern Brazil. *Sci Rep* 2018;**8**:16315. https://doi.org/10.1038/s41598-018-34630-1

Szretter KJ, Daniels BP, Cho H *et al.* 2′-O methylation of the viral mRNA cap by West Nile virus evades Ifit1-dependent and -independent mechanisms of host restriction In vivo. *PLoS Pathog* 2012;**8**:e1002698. https://doi.org/10.1371/journal.ppat.1002698

Temmam S, Bigot T, Chrétien D *et al.* Insights into the host range, genetic diversity, and geographical distribution of jingmenviruses. *mSphere* 2019;**4**:e00645–19. https://doi.org/10.1128/mSphere.00645-19

Villa, Erika C, Maruyama Sandra R, de Miranda-Santos Isabel KF *et al.* Complete coding genome sequence for Mogiana tick virus, a Jingmenvirus isolated from ticks in Brazil. *Genome Announc* 2017;**5**:10–1128. https://doi.org/10.1128/genomeA.00232-17

Wang ZD, Wang W, Wang NN *et al.* Prevalence of the emerging novel Alongshan virus infection in sheep and cattle in Inner Mongolia, northeastern China. *Parasit Vectors* 2019a;**12**:450. https://doi.org/10.1186/s13071-019-3707-1

Wang Z-D, Wang B, Wei F *et al.* A new segmented virus associated with human febrile illness in China. *N Engl J*

Med 2019b;**380**:2116–25. https://doi.org/10.1056/NEJMoa1805068

Wang X, Jing X, Shi J *et al.* A jingmenvirus RNA-dependent RNA polymerase structurally resembles the flavivirus counterpart but with different features at the initiation phase. *Nucleic Acids Res* 2024;**52**:3278–90. https://doi.org/10.1093/nar/gkae042

Wikel SK. Ticks and tick-borne infections: complex ecology, agents, and host interactions. *Vet Sci* 2018;**5**:60. https://doi.org/10.3390/vetsci5020060

Wu Z, Zhang M, Zhang Y *et al.* Jingmen tick virus: an emerging arbovirus with a global threat. *mSphere* 2023;**8**:e00281–23. https://doi.org/10.1128/msphere.00281-23

Yang J, Jing X, Yi W *et al.* Crystal structure of a tick-borne flavivirus RNA-dependent RNA polymerase suggests a host adaptation hotspot in RNA viruses. *Nucleic Acids Res* 2021;**49**:1567–80. https://doi.org/10.1093/nar/gkaa1250

Yu Z-M, Chen J-T, Qin J *et al.* Identification and characterization of Jingmen tick virus in rodents from Xinjiang, China. *Infect Genet Evol* 2020;**84**:104411. https://doi.org/10.1016/j.meegid.2020.104411

Zhang X, Wang N, Wang Z *et al.* The discovery of segmented flaviviruses: implications for viral emergence. *Curr Opin Virol* 2020;**40**:11–8. https://doi.org/10.1016/j.coviro.2020.02.001

Züst R, Cervantes-Barragan L, Habjan M *et al.* Ribose 2'-O-methylation provides a molecular signature for the distinction of self and non-self mRNA dependent on the RNA sensor Mda5. *Nat Immunol* 2011;**12**:137–43. https://doi.org/10.1038/ni.1979

Virus Evolution, 2025, 1–15
https://doi.org/10.1093/ve/veaf045
Research Article